Available online at www.sciencedirect.com
SCIENCE DIRECT®
Journal of Nuclear Materials 320 (2003) 85–95
journal of nuclear materials
www.elsevier.com/locate/jnucmat

Microstructure characterisation of irradiated Am-containing $MgAl_2O_4$ (EFTTRA-T4)

T. Wiss *, R.J.M. Konings, C.T. Walker, H. Thiele

European Commission, Joint Research Centre, Institute for Transuranium Elements, P.O. Box 2340, Karlsruhe D-76125, Germany

Abstract

The first americium-containing inert matrix target ($MgAl_2O_4$) irradiation in the High Flux Reactor (Petten) in the EFTTRA-T4 experiment has demonstrated the feasibility of transmutation of minor actinides in a once through scenario in a epi-thermal neutron flux. The inert matrix itself showed rather poor behaviour under irradiation. A large swelling linked to a high porosity formation was observed. Scanning and transmission electron microscopy were used to investigate the radiation damage from the fission products and alpha-decay. It was observed that $MgAl_2O_4$ undergoes severe structural modifications such as amorphisation. Electron probe microanalysis revealed that the target was not stable from a chemical aspect implying that its use as a target for transmutation may need to be reconsidered.

1. Introduction

During operation, nuclear UO_2 fuel generates transuranium elements, mainly Pu isotopes but also minor actinides (MA) such as Am and Cm by neutron capture and radioactive decay processes. These radionuclides contribute greatly to the radiotoxicity of spent nuclear fuel. To reduce the radiotoxic inventory of spent nuclear fuel, the long lived transuranium elements should be transmuted into stable or short lived elements. In the actual scenario of fuel reprocessing (separation of the fission products and of U and Pu through, e.g., the PUREX process) additional steps to separate the minor actinides from the lanthanides could be envisaged via liquid–liquid extraction (e.g., DIAMEX process [1]) or via pyro-reprocessing [2,3]. The separated minor actinides would then be incorporated in a uranium-free matrix (inert matrix fuel, IMF) and transmuted through nuclear reactions (fission and neutron capture). The choice of such a matrix depends on various parameters among them the thermophysical properties, the mechanical stability and the radiation resistance to the various damaging sources (neutrons, fission, alpha-decay) [4]. Many different transmutation schemes have been envisaged [5,6] paying attention to the material properties, the neutronic aspects of dedicated transmutation devices (e.g., energy of the neutrons vs. capture cross-sections) and reprocessing feasibility. In these various concepts the transmutation device could be a fast neutron reactor (FNR) or an accelerator driven system (ADS) and the radiotoxic nuclide could be transformed in a once through or in multi-recycling schemes.

The EFTTRA-T4 [1] experiment aimed at demonstrating the feasibility of a specific transmutation scheme, i.e., a once through scenario consisting of the transmutation of ^{241}Am in an inert matrix target. Magnesium aluminate spinel was selected during the

* Corresponding author. Tel.: +49-7247 951 447; fax: +49-7247 951 199.
E-mail address: wiss@itu.fzk.de (T. Wiss).

[1] Experimental feasibility of targets for transmutation (EFTTRA) is a network of research organizations in France (EdF and CEA), Germany (JRC-ITU and FzK), and the Netherlands (JRC-IE and NRG).

0022-3115/03/$ - see front matter
doi:10.1016/S0022-3115(03)00174-0

design phase of the experiment (1994) because of its promising behaviour in neutron radiation fields [7]. $MgAl_2O_4$ pellets were fabricated and infiltrated with ~12 wt% of Am [8]. The target was irradiated in the HFR and the first post-irradiation examinations (PIE) were performed at NRG and ITU [9]. Non-destructive examinations, such as gamma tomography, profilometry, X-ray radiography and gas puncturing were carried out on the irradiated capsule and ceramography was carried out on the irradiated material. The most notable observations were the large swelling of the matrix (~18%) and the formation of considerable porosity (~15%). The post-test calculations using the MCNP and FISPACT codes predicted 94.3% of the ^{241}Am content had transmuted of which 27.9% had occurred by neutron fission.

The behaviour of $MgAl_2O_4$ against the impact of neutrons, alpha-particles, and recoil atoms and fission products has been investigated extensively in separate effect studies. It was shown that the material remains stable under neutron irradiation up to high fluences [10–13], that alpha-particles lead to low damage formation [14,15] but that fission products might amorphise the material inducing significant swelling [16–19]. In addition, the production of helium from the alpha-decaying actinides in the EFTTRA-T4 experiment was considerable. This explains the significant porosity observed. Thus the radiation stability of $MgAl_2O_4$ for each damaging source was studied separately. The concomitant effects of the different damaging sources in this in-pile irradiated target has been studied by transmission electron microscopy (TEM), by scanning electron microscopy (SEM) and by wave length dispersive (WDX) electron probe microanalysis (EPMA). The aim of the examinations performed was to acquire information on the inert matrix microstructure and chemical state after irradiation. This included:

- The crystallographic state of the matrix following damage accumulation.
- The location of fission gases and helium.
- The location of fission products.
- The evolution of the original Am containing inclusions.
- The mechanical behaviour of the material during irradiation.

2. Experimental

Sample fabrication, irradiation conditions, neutron metrology, burn-up calculations, non-destructive examinations, gas puncturing and ceramography data were presented extensively in a previous paper [9]. In summary, the EFTTRA-T4 samples were prepared by infiltration of porous $MgAl_2O_4$ pellets with an americium nitrate solution according to the methods described in [20]. The porous pellets were prepared from a commercial powder (Baikalox S33CR, Baikowski Chemie), granulated and compacted at a pressure of 390 MPa using a bi-directional press. The pellets were placed in batches (up to 12) on a perforated teflon tray, which was lowered slowly into an Am nitrate solution, prepared by dissolving americium oxide in nitric acid and concentrated to an Am metal content of approximately 400 g/l. Upon withdrawal the pellets were dried, and then calcined at 700 °C for 4 h under Ar/H_2 before being sintered at 1650 °C under the same atmosphere. The Am-content in the pellets was found to vary between 9.7 and 11.9 wt%, the mean value being (11.1 ± 0.7) wt%.

The irradiation of the EFTTRA-T4 capsule containing 10 Am-infiltrated $MgAl_2O_4$ pellets was performed between August 1996 and November 1997 and lasted 358.42 full power days. The temperature of the capsule surface was monitored by surrounding thermocouples and was maintained at around 400 °C by using an adjustable He–Ne mixture in the second containment wall. The flux distribution and neutron fluence were measured by gamma-scanning wires and neutron fluence detectors positioned around the capsule. The cumulative fast neutron fluence ($E > 0.1$ MeV) was 1.67×10^{26} m^{-2} and the neutron fluence profile was flat along the target stack.

For the studies reported in this paper, disks from the irradiated target were cut and the ceramic material extruded from the cladding material. Larger fragments of the inert matrix were observed on a Philips XL40 SEM mounted inside a glove-box. Selected pieces were annealed at 1180, 1330, 1780 and 1980 °C and subsequently analysed by SEM. Secondary electron (SE) images and backscattered electron (BSE) images were recorded as well as energy dispersive X-ray (EDX) spectra and single element distribution maps.

To provide electron-transparent specimens for TEM investigations, small fragments of the material were crushed in ethanol. A droplet of the resulting suspension was deposited on a copper TEM grid coated with graphite. The TEM used in this study was a HITACHI STEM H700HST modified to allow handling of radioactive materials. Scanning transmission electron microscopy (STEM), TEM, selective area electron diffraction (SAED) and EDX microbeam analysis were performed on the irradiated material.

WDX EPMA was performed on a polished section of the irradiated target using the Institute's shielded electron probe microanalyser. Point analysis and area analysis using a 300×300 μm raster were performed. Point analysis was used to determine the local composition of the $MgAl_2O_4$ matrix, whereas area analysis was used to determine the bulk composition of the material including any second phases. The conventional

Table 1
WDX EPMA analysis conditions used for the EFTTRA-T4 sample

Element	X-ray line	Diffracting crystal	E_0 (keV)	Beam current (nA)	Standard
Al	$K\alpha_1$ (2)	TAP	25	100	Al
Mg	$K\alpha_1$	TAP	25	100	Mg
Pu	$M\beta_1$	Quartz $10\bar{1}1$	25	100	PuO_2
Am	$M\beta_1$	Quartz $10\bar{1}1$	25	100	AmO_2
Nd	$L\alpha_1$	LiF	25	100	Nd
Cs	$L\beta_1$	LiF	25	100	CsI
Xe	$L\alpha_1$	Quartz $10\bar{1}1$	25	100	Sb[a]

[a] See text Section 2.

microprobe matrix correction was made using the PAP [21] option in the XMAS program marketed by SAMX, France. Table 1 summarises the experimental conditions used for the EPMA analysis. For Xe, Sb was used as a standard and a correction factor applied to the intensity of the Sb Lα line. The correction factor (1.34) was derived by interpolating the intensity of the Lα X-ray line for pure solid Xe from the intensities from adjacent elements in the Periodic Table. A more detailed description of the procedure can be found in Ref. [22].

The TEM and EPMA investigations were performed 4 years after the end of irradiation (EOI). The actinide composition of the target at this time (EOI + 4 years) was calculated by the NUCLIDE.NET code [23] from the composition at EOI given by the MCNP/FISTPAC codes [24]. Table 2 shows the actinide composition deduced from the total inventory calculated. Pu isotopes constituted more than 75% of the actinides present after 4 years cooling. During cooling a large part of ^{242}Cm underwent alpha-decay to ^{238}Pu explaining on one hand the increase of Pu and on the other the production of

Table 2
Calculated actinide composition at the end of irradiation (EOI) and after 4 years cooling

Isotope	Composition, atom percent of the total actinides	
	EOI	EOI + 4 years
^{234}U	0.52	1.64
^{235}U	0.04	0.04
^{236}U	0.00	0.00
Total U	0.56	1.68
^{237}Np	0.04	0.07
Total Np	0.04	0.07
^{238}Pu	50.34	53.43
^{239}Pu	9.01	9.15
^{240}Pu	2.03	2.74
^{241}Pu	1.96	1.73
^{242}Pu	9.68	9.69
Total Pu	73.02	76.67
^{241}Am	5.40	5.61
^{242}Am	0.06	0.06
^{243}Am	7.18	7.17
Total Am	12.64	12.84
^{242}Cm	4.28	0.01
^{243}Cm	1.25	1.17
^{244}Cm	7.42	6.70
^{245}Cm	0.59	0.59
^{246}Cm	0.19	0.19
Total Cm	13.73	8.72

large quantities of helium during storage. The amount of helium produced after irradiation was about 2.4 mg g^{-1} of target and 4 mg g^{-1} at the time TEM and EPMA were performed.

3. Results

3.1. SEM and EDX microbeam analysis

The examination of the EFTTRA-T4 target by SEM confirmed the high porosity observed by ceramography (average $\sim$ 18% compared with the initial 3% of the as-fabricated material). The porosity even increased to 40% in the 350 μm wide shell with higher ^{241}Am content at fabrication [9]. This area can be seen on the left part of the SEM micrograph Fig. 1(a). Metallic fission product precipitates containing Mo, Tc, Ru, Rh, and Pd and with sizes up to 2 μm (see Fig. 1(b)) were distributed all over the specimen as confirmed by EDX analysis. The matrix appears to be constituted of small ($\sim$500 nm) grains embedded in a metamict phase (see Fig. 1(b) and (c)). Bright areas surrounding the pores but also evenly distributed in the matrix were observed. EDX analysis showed that they were rich in Pu and Al. The inhomogeneous distribution of the Pu can be seen on the SEM micrograph Fig. 1(c) (brighter areas surrounding pores). This could also be clearly discerned in the BSE mode which gives a strong contrast proportional to the average atomic number of the constituent elements in the analysed area as shown in Fig. 1(d) (grey areas). The Pu is mainly composed of the isotope ^{238}Pu formed solely by the radioactive decay of ^{242}Cm produced from neutron capture by the original ^{242}Am content in the matrix. The picture therefore reveals the original Am distribution i.e., in the form of 2–3 μm inclusions. The range of the recoil atoms from alpha-decaying ^{242}Cm and ^{238}Pu being of about 20 nm, the newly formed actinides have remained within the circumference of the original Am inclusions.

3.2. Wavelength dispersive EPMA

WDX EPMA was performed on an irradiated disk section. The distribution of the matrix atoms (Mg, Al), of Am and Pu, of the fission gas Xe and fission products

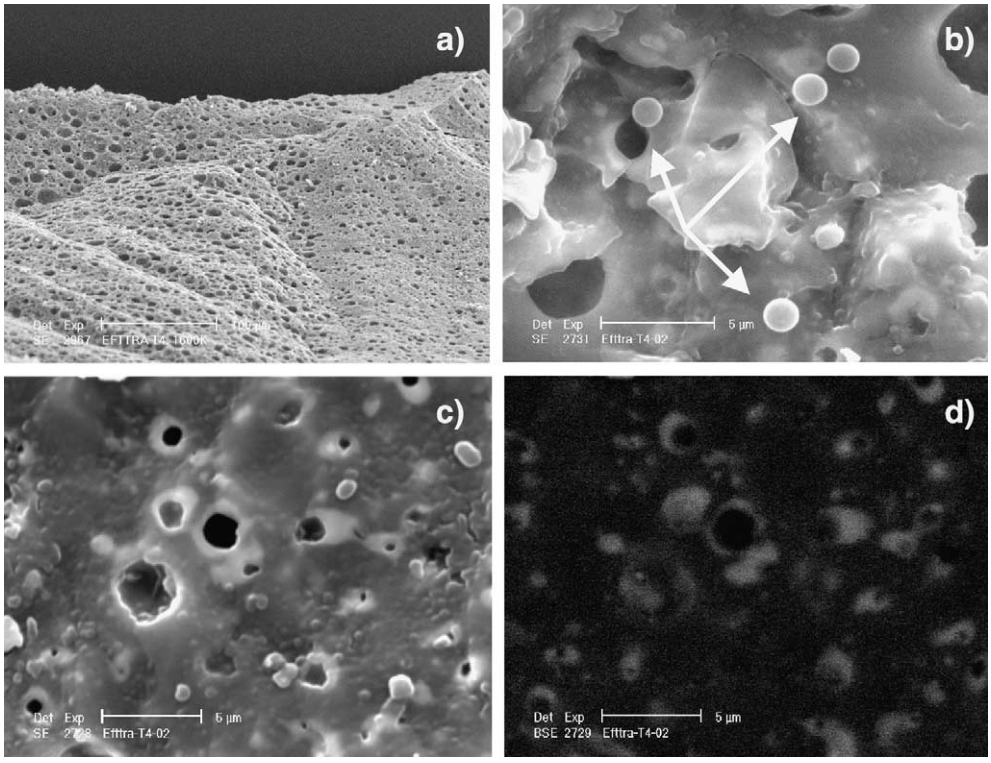

Fig. 1. SEM micrographs of the EFTTRA-T4 target. (a) The high porosity after irradiation. The region of higher porosity on the left corresponds to a 350 μm wide band which contained an increased concentration of Am (14 wt%), (b) metallic fission product inclusions of Mo, Tc, Ru, Rh, Pd indicated by arrows, (c) enlarged micrograph of the porosity showing a Pu-containing phase surrounding the pores as revealed by the bright areas in the backscattered electron image in (d).

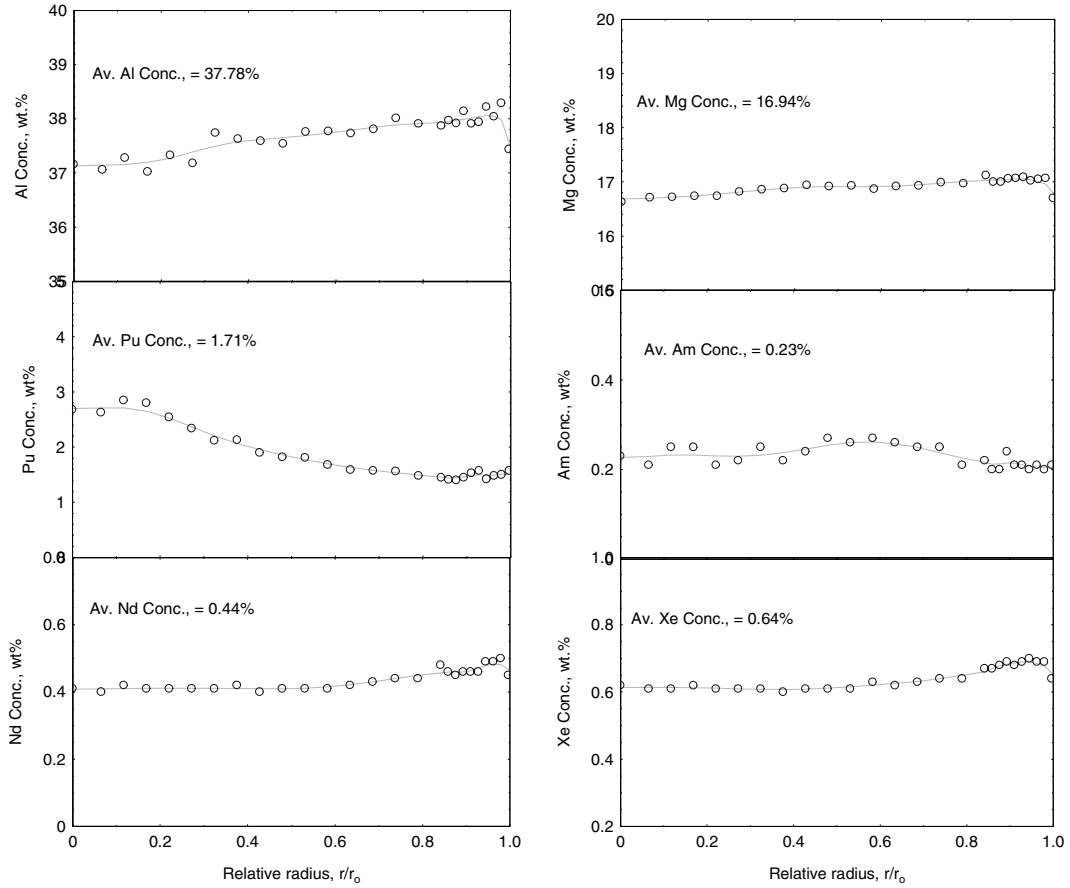

Fig. 2. Radial distribution of Al, Mg, Pu, Am, Nd and Xe in the EFTTRA-T4 target sample measured by WDX EPMA.

Nd and Cs was recorded along a radius of the disk. Fig. 2 shows the Pu, Am, Nd and Xe profiles recorded by point analysis of the matrix. The Nd and Xe profiles are flat with an anticipated slight increase towards the surface attributed to a higher local fission rate. It is pointed out that the disparity in Fig. 2 between the Pu matrix profile, which shows an increase in Pu concentration in the central region of the pellet, and the fission products profiles represented by Nd and Xe, which are fairly flat, is an apparent one only. The different trends can be explained if it is recognised that only 20% of the Pu present is fissile and the additional fission product content resulting from the fission of Pu in the $MgAl_2O_4$ matrix is within the scatter band of the EPMA results. It is assumed that the increase in Pu concentration measured in the matrix results from diffusion out of the actinide inclusions. This is supported by the fact that Pu inclusions in the centre of the fuel contain substantially less Pu than those at other radial location (see Table 3).

WDX EPMA also revealed that a Pu-containing second phase whose Pu content and relative concentration varied radially was present in the target. Area analysis however, revealed that the bulk composition of the material was quite uniform. The following concentrations were measured: Pu 6.13 ± 0.01 wt%, Am 0.47 ± 0.01 wt%, Nd 0.43 ± 0.01 wt%, Cs 0.30 ± 0.02 wt% and Xe 0.58 ± 0.01 wt%. It is pointed out that area analysis results reported above have not been corrected for porosity. It is assumed that such a correction would increase the measured concentrations by up to 15% and more, depending on the local porosity value in the area analysed, the electron penetration depth and the mass absorption coefficient of the characteristic X-ray line in the $MgAl_2O_4$ spinel phase (see Fig. 3). Fig. 3 contains electron absorption micrographs of the fuel structure at the surface, mid-radius and centre of the EFTTRA-T4 pellet. It is evident that with increasing distance from the pellet surface the pores dispersed in the spinel matrix increase in size and decrease in number.

The EPMA area analysis results are compared with the concentrations predicted with the MCNP and FISPACT codes in Table 4. The comparison is based on

Table 3
WDX EPMA results for the composition of a second phase dispersed in the matrix of sample EFTTRA-T4

Location	Concentration (wt%)								
	Mg	Al	Xe	Cs	Nd	Pu	Am	O[a]	Σ
	7.89	28.55	0.95	0.23	0.61	19.58	1.5	40	99.31
Surface	7.81	29.56	0.84	0.21	0.59	19.49	1.31	40	99.81
	7.78	28.53	0.83	0.22	0.58	20.79	1.64	40	100.37
	9.54	30.39	0.98	0.24	0.72	17.65	1.35	40	100.87
Mid radius	13.23	25.45	0.75	0.21	0.65	18.34	1.22	40	99.85
	11.11	28.37	1.01	0.19	0.64	17.73	1.28	40	100.33
	10.47	32.57	0.97	0.21	0.47	13.16	0.88	40	98.73
Centre	12.18	32.89	0.97	0.18	0.52	10.68	0.84	40	98.26
	12.53	33.65	0.95	0.17	0.44	9.33	0.88	40	97.95

[a] Hypothetic concentration which when inserted in the matrix correction program gives approximately 100 wt% when the concentration of all elements are summed.

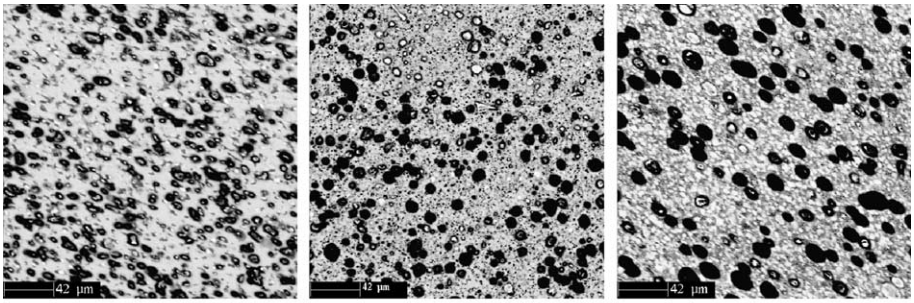

Fig. 3. Absorbed electron images of the porosity at the surface, mid-radius and centre of an EFTTRA-T4 pellet.

Table 4
Comparison between the measured (WDX-EPMA) and calculated (MCNP/FISPACT) element analysis

	Pu/Am_{ini}[a]	Am/Am_{ini}	Am/Pu	Nd/Pu	Xe/Pu	Cs/Pu
EPMA	0.50	0.04	0.08	0.12	0.17	0.09
MCNP/FISPACT	0.56	0.08	0.16	0.08	0.14	0.06

[a] Am_{ini} is the initial americium content.

the mass concentration ratios of the measured elements with the addition of the initial Am concentration for completeness. It is evident from the close similarity in the measured and predicted ratios that the actinide and fission concentrations predicted with the MCNP and FISPACT codes are in reasonable agreement with the experimental results. A further important observation from the ratios listed in Table 4 is that the measured Pu and Am concentrations are lower, and the measured fission product concentrations are higher than the calculated values, implying that the burnout of the target might be higher than calculated.

Table 3 lists the point analysis results for the Pu-containing second phase at three radial positions. It is seen from the table that the composition of the phase varies across the pellet radius. The Pu content of the phase decreases markedly with distance from the target surface from about 20 to 11 wt% in the pellet centre. It is also evident that in the outer region of the target the phase contains markedly less Mg (7.8 wt% compared with around 11.5 wt% in the mid and central regions). It is pointed out that the analysis results correspond to the composition of no known ceramic phase.

3.3. TEM and STEM

The plutonium containing phase(s) surrounding the pores could be well observed. This phase was located at the sites of the original Am-inclusions. The porosity developed inside of the inclusions and grew with gas build-up. Fig. 4 shows such a pore surrounded by a Pu-rich phase. On the same micrograph, bubbles associated with fission product inclusions are also seen (indicated by arrows). It is to be noted that the boundary between the Pu-rich phase and the matrix (Mg–Al phase) is sharp indicating no inter-diffusion in the analysed area. However, small plutonium-rich inclusions were found in the matrix not associated with porosity.

TEM investigations also revealed that the $MgAl_2O_4$ matrix had recrystallized in nanometer sized grains. Fig. 5 shows three TEM micrographs representative of the material. Fig. 5(a) is a view of the Pu-rich phase with some gas bubbles associated with FPs inclusions. Fig. 5(b) and (c) reveal the nano-grain structure of the matrix.

The selective area electron diffraction (SAED) patterns that accompany the TEM micrographs in Fig. 5(a)–(c) revealed a complex phase distribution in the EFTTRA-T4 matrix. From the diffraction rings and from the calibration of the camera length with an Al standard ($L = 296.8$ mm nm^{-1}) peak positions were deduced and the corresponding d-spacing calculated by using the 'ProcessDiffraction' software [25]. For the purpose of comparison, Fig. 5(d) shows the microstructure and SAED pattern of an $MgAl_2O_4$ single crystal, nano-recrystallized from an amorphous state obtained by irradiation with 70 MeV I-ions [19]. The d-spacing deduced from the four SAED patterns could partially be assigned to $MgAl_2O_4$. The main difference between the patterns appears to be reflections of lower intensity in the different areas of the EFTTRA-T4 material examined. Contributions from segregated phases from the $MgAl_2O_4$ (MgO, Al_2O_3) or of known compounds like PuO_2, $PuAlO_3$ could not be identified. Fig. 6(a) shows a STEM image of an area where two types of phases are neighbouring. A Pu-rich phase about 300 nm wide surrounding a pore and presenting a nano-grain structure is shown next to a restructured Mg–Al-rich phase. An EDX line scan (Fig. 6(b)) recorded over the Pu-phase and matrix clearly reveals the different chemical composition of the two phases. The signals of Pu, Al and Mg are plotted in counts. It can be seen that the Pu and Mg signals are well segregated. The Pu-phase is seen to contain a high concentration of aluminium. Electron diffraction and imaging reveal that this phase could be amorphous or in the form of a nano-crystalline phase. STEM imaging and EDX measurements also showed the presence of plutonium–aluminium inclusions in the matrix. Fission product inclusions were also detected in the matrix.

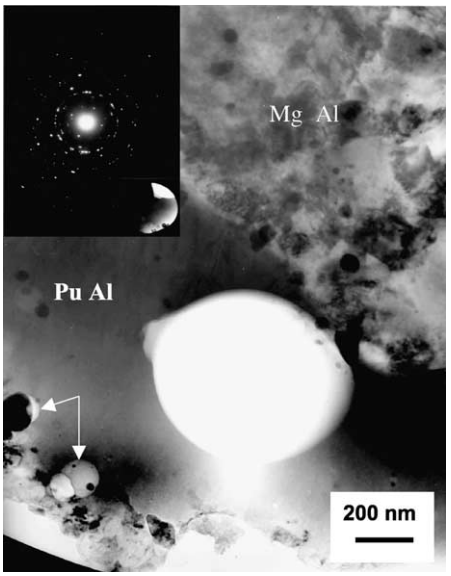

Fig. 4. TEM micrograph showing a Pu–Al-rich phase surrounding a large bubble produced by He precipitation and presumably bubble coalescence. The $MgAl_2O_4$ matrix, indicated as Mg–Al has transformed to a microstructure of nanocrystals. The arrows indicate small gas bubbles associated with fission product inclusions (as observed in conventional UO_2 fuel). The inset, upper left, shows a complex diffraction pattern attributed to the co-existence of several phases.

In summary, the $MgAl_2O_4$ matrix was composed of small grains between a few tens of nanometers and one micrometer in size compared with the original grain size of 10 μm. Fission product inclusions of noble metals were observed often associated with gas bubbles. The size of the fission product inclusions ranged between a few nanometers to some micrometers.

4. Discussion

The post-irradiation examinations reported in this paper aimed at answering open questions concerning the microstructure evolution of a $MgAl_2O_4$ inert matrix during irradiation. It will be demonstrated that the inert matrix became amorphous prior to its recrystallization during storage.

A significant swelling of about 17% on average had occurred in this transmutation target. The SEM and WDX EPMA investigations confirmed the high porosity of the material after irradiation. It was previously shown that large pores with sizes up to 10 μm were formed in the material and that only 20% of the helium and 5% of the fission gases formed were released during reactor operation. The average porosity was 15%, which is slightly less than the measured swelling of 18%.

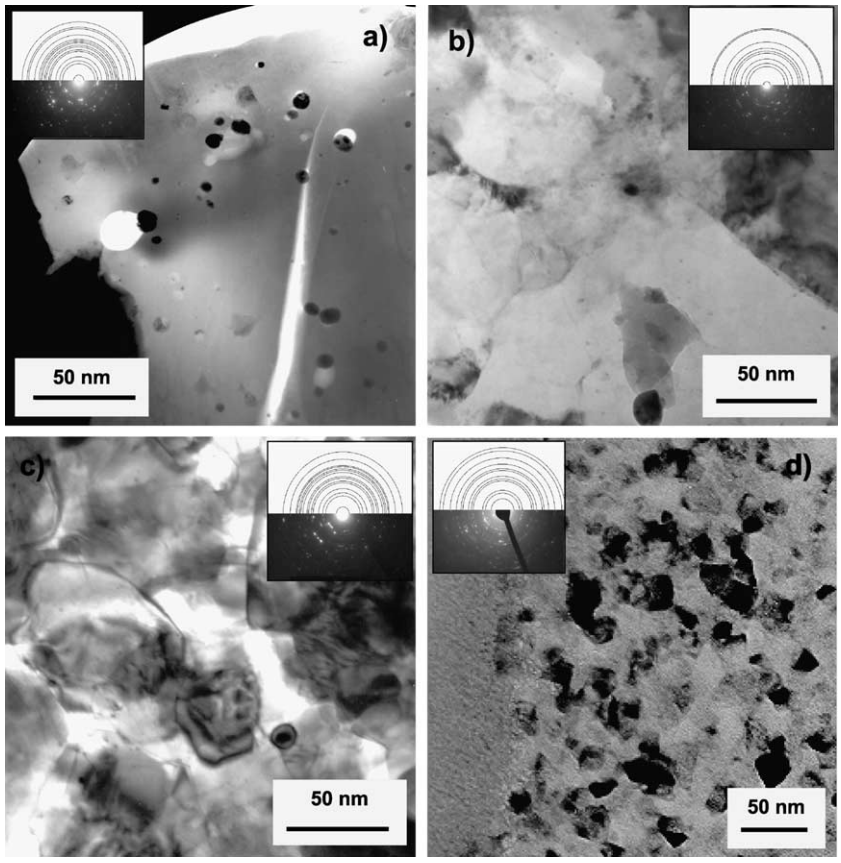

Fig. 5. TEM bright field images and associated SAEDs with the calculated half circles of (a) a Pu–Al-rich phase, (b) and (c) nano-sized spinel grains in the EFTTRA-T4 target, (d) nano-recrystallized grains in an ion-irradiated induced amorphous $MgAl_2O_4$.

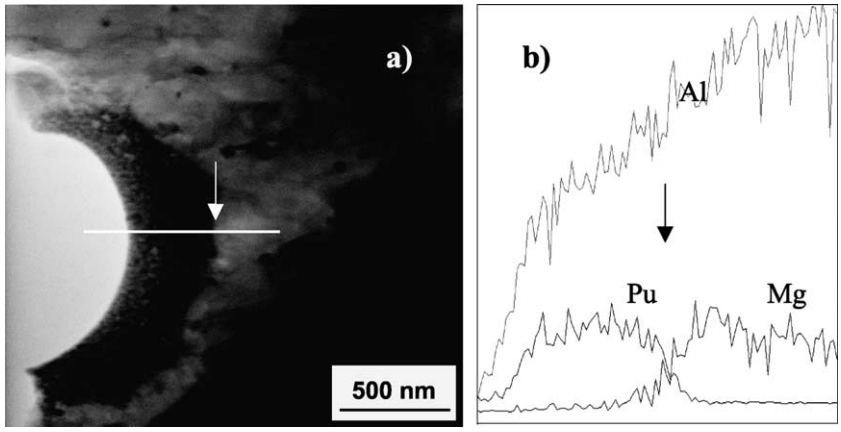

Fig. 6. (a) STEM micrograph showing from the left to the right a pore, an area of Pu–Al oxide-rich phase and the $MgAl_2O_4$ matrix, (b) EDX line scans for Al, Pu and Mg across the the Pu–Al-rich phase and into the $MgAl_2O_4$ matrix. The white line on the STEM micrograph marks the location of the recorded EDX line scan.

Laboratory radiation damage studies have demonstrated that $MgAl_2O_4$ can become amorphous when irradiated with fission products of fission energy, such as 70 MeV iodine ions, as shown in Ref. [19]. As a

macroscopic effect of amorphisation, swelling as high as 15% was observed for ion irradiations at 500 °C and about 7% at 900 °C [18]. The EFTTRA-T4 target did not show direct evidence for amorphisation. However, the observed nano-grains were presumably formed from an amorphous state as observed in ion-irradiated $MgAl_2O_4$. In that case recrystallization occurred rapidly under the TEM electron beam. This is also known to occur in other materials (e.g., $Gd_2Ti_2O_7$ pyrochlores [26]). For the EFTTRA-T4 material, it may be assumed that the high beta dose accumulated from the decaying fission products over 4 years of storage has produced the same effect. Another observation in support of the recrystallization of the target during storage is that the $MgAl_2O_4$ matrix grains are defect free and contain few gas bubbles in contrast to the Pu-rich phase. On the basis of ion implantation studies, where it was shown that xenon is not mobile in amorphous $MgAl_2O_4$ below 1100 °C [27], it can be argued that during recrystallization the gas has been swept out from the $MgAl_2O_4$ matrix. In the same study of Xe-implanted $MgAl_2O_4$ it was shown that amorphous $MgAl_2O_4$ recrystallizes between 625 and 850 °C. If this is so, recrystallization of the EFTTRA-T4 is unlikely to have been thermally driven because the central temperature during irradiation probably did not exceed 650 °C at EOI. Additionally, in the THERMHET irradiation i.e., micro-dispersed UO_2 in $MgAl_2O_4$, it was shown that the $MgAl_2O_4$ matrix experienced a swelling of 24% [28]. XRD analysis revealed that the matrix was amorphous [29,30]. As no significant quantities of helium were formed the swelling was explained by fission damage causing amorphisation at low temperature between the irradiation cycles. In the EFTTRA-T4ter experiment, a $MgAl_2O_4$ target with micro-dispersed UO_2 fissile inclusions was irradiated for 652 EFPD leading to a swelling of ~12% [31]. Also for this target the major factor for swelling is attributed to the damage caused to the matrix (amorphisation).

The damage formed in the matrix of the EFTTRA-T4 target was calculated using the SRIM 2000 code [32]. It was found that fission caused about 180 displacements per atom (dpa), neutrons ~17 dpa and alpha-decays ~1 dpa, summing to about 200 dpa. When the initial microstructure is considered, i.e., the size and distribution of the Am containing inclusions, it is apparent that the whole matrix was subjected to fission damage [33]. This finding is important for understanding the mechanisms of damage ingrowth and microstructure change of the matrix. It is however, not the purely elastic collisions of the fission products, which result in displacements of the target lattice atoms, that are mainly responsible for the transformation of the $MgAl_2O_4$ microstructure, but rather the fission spikes. As an indication, the total number of fissions in EFTTRA-T4 was around 1.4×10^{20} per cm^{-3}. The ion-irradiated $MgAl_2O_4$ for which amorphisation attributed to high electronic energy deposition was observed [19], received an equivalent fission density of more than one order of magnitude lower. As the post-irradiation examination of the EFTTRA-T4 target was carried out 4 years after the end of the irradiation, damage accumulated in the material from the alpha-decay during storage has also been considered. In a previous investigation it was shown that $MgAl_2O_4$ is only slightly affected by the alpha-particle damage [34]. In the EFTTRA-T4 target the alpha-decaying actinides were concentrated in inclusions of 2–3 μm leading to the conclusion that recoil atoms from alpha-decay will have affected only a thin shell (15 nm) around the inclusions and that during storage damage to the $MgAl_2O_4$ matrix from alpha-particles was negligible.

Ceramography of the EFTTRA-T4 pellets revealed radial cracks which were attributed to the thermal stress field during cooling when the target material was bonded to the cladding. The same observation was found in the THERMHET material. TEM analysis of the EFTTRA-T4 target did not reveal the presence of dislocations. In view of the high target swelling and the associated development of gas pores, the absence of any mechanical induced defects/stress indicates that the material behaved plastically. This would be expected if the matrix had been amorphous and subsequently recrystallized.

By considering the above-mentioned aspects of porosity formation, amorphisation and mechanical behaviour, a mechanism for pore formation can be postulated. If it is accepted that alpha-decay contributes to the damage of the actinide inclusions, it is probable that large numbers of point defects (Frenkel pairs) were created in these inclusions. Vacancies acted as sinks for the helium produced from the neighbouring inclusions. The separation between inclusions was about 10 μm, which corresponds to the range of the 5–6 MeV alpha-particles. Bubble growth occurred easily in the matrix which behaved plastically.

The structure of the recrystallized matrix is not known with certainty. It is assumed that during fabrication the Am forms a perovskite phase with Al of type $AmAlO_3$ [20]. As a result depletion of Al in the $MgAl_2O_4$ matrix should have occurred. WDX EPMA of the irradiated material revealed that the concentration of Al in the actinide inclusions was much higher than in the perovskite phase (25–34 wt% compared with 8.5 wt%). The $MgAl_2O_4$ structure can, however, diverge from stoichiometry [35] or present inversion of the cation positions [36], the resulting compounds having different lattice parameters. Indexing of the SAED patterns from TEM is therefore uncertain, but the patterns were similar to those for ion irradiated $MgAl_2O_4$. However, the EFTTRA-T4 material presents a wide palette of secondary phases mainly in the vicinity of the

large pores. It was shown that these phases could be either amorphous or crystalline and that their chemical composition varies. It was also found that smaller Pu-rich inclusions were present in the matrix. From the WDX EPMA and EDX analyses it is postulated that the actinide inclusions could contain a $MgPuAl_{11}O_{19}$ hibonite phase which has been identified by Japanese researchers [37].

5. Summary and conclusion

The microstructure of a Am-doped $MgAl_2O_4$ target used for Am transmutation in a high thermal flux reactor has been investigated. The matrix was probably amorphous at the end of the irradiation and to have recrystallized during storage. Large pores, but also bubbles, formed in the matrix mainly from helium resulting from alpha-decay during storage, and from the fission gases produced during irradiation. Fission products were distributed throughout the matrix and five-metal precipitates were found in the matrix often associated with gas bubbles. The original Am-inclusions had transformed into Pu-rich inclusions which are possibly based on a hibonite phase of the type $MgPuAl_{11}O_{19}$. WDX EPMA also revealed that the burnout of the target might be slightly higher than predicted by calculation.

Since the $MgAl_2O_4$ matrix shows a pronounced plastic deformation associated with a large swelling it should no longer be considered as a candidate micro-dispersed inert matrix for actinide transmutation. Its unpredictable behaviour is linked to its poor chemical stability when used in conjunction with americium and its transmutation products, and its predilection to amorphise under reactor irradiation conditions.

Acknowledgements

The authors wish to express their thanks to E. Lazarus and S. Hollas for sample preparation in the hot cells and W. Ziehl and S. Bremier for the WDX EPMA analysis.

References

[1] C. Madic, P. Blanc, N. Condamines, P. Baron, L. Berthon, C. Nicol, C. Pozo, M. Lecomte, M. Philippe, M. Masson, C. Hecquet, M.J. Hudson, in: Fourth International Conference on Nuclear Fuel Reprocessing and Waste Management, RECOD'94, London, UK, vol. 2, 1994.

[2] A.V. Bychkov, S.K. Vavilov, O.V. Skiba, P.T. Porodnov, A.K. Pravdin, G.P. Popkov, K. Suzuki, Y. Shoji, T. Kobayashi, in: GLOBAL'97, Yokohama, Japan, vol. 2, 1997, p. 912.

[3] T. Inoue, H. Tanaka, in: International Conference on Future Nuclear Systems, GLOBAL'97, Yokohama, Japan, vol. 1, 1997, p. 646.

[4] H. Matzke, V.V. Rondinella, T. Wiss, J. Nucl. Mater. 274 (1999) 47.

[5] J. Magill, P. Peerani, J. van Geel, in: International Workshop on the Physics of Accelerator-Driven Systems for Nuclear Transmutation and Clean Energy Production, Trento, Italy, 1997.

[6] C. Rubbia, CERN concept of ADS, in: I.A.E.A. Technical Commitee Meeting on Feasibility and Motivation for Hybrid Concepts for Nuclear Energy Generation and Transmutation, Madrid, Spain, 1997.

[7] J.-F. Babelot, R. Conrad, R.J.M. Konings, G. Mühling, M. Salvatores, G. Vambenepe, J. Alloys Comp. 271 (1998) 606.

[8] A. Fernandez, K. Richter, J. Somers, J. Alloys Comp. 271 (1998) 616.

[9] R.J.M. Konings, R. Conrad, G. Dassel, B. Pijlgroms, J. Somers, E. Toscano, J. Nucl. Mater. 282 (2000) 159.

[10] F.W. Clinard, G.F. Hurley, L.W. Hobbs, J. Nucl. Mater. 108 (1982) 655.

[11] F.W. Clinard, G.F. Hurley, L.W. Hobbs, D.L. Rohr, R.A. Youngman, J. Nucl. Mater. 141 (1984) 1386.

[12] K. Sickafus, A.C. Larson, Y.M. Nastasi, G.W. Hollenberg, F.A. Garner, R.C. Bradt, J. Nucl. Mater. 219 (1995) 128.

[13] R.J.M. Konings, K. Bakker, J.G. Boshoven, R. Conrad, H. Hein, J. Nucl. Mater. 254 (1998) 135.

[14] A. Turos, E. Falcone, A. Drigo, A. Sambo, H. Matzke, Nucl. Instrum. and Meth. B 115 (1996) 359.

[15] S.J. Zinkle, J. Nucl. Mater. 219 (1995) 113.

[16] S.J. Zinkle, V.A. Skuratov, Nucl. Instrum. and Meth. B 141 (1998) 737.

[17] S.J. Zinkle, V.A. Skuratov, H. Matzke, in: MRS Symposium Proceedings, Materials Research Society, Warrendale, PA, 1999, p. 299.

[18] T. Wiss, H. Matzke, Radiat. Meas. 31 (1999) 507.

[19] T. Wiss, H. Matzke, V.V.R. Rondinella, T. Sonoda, W. Assmann, M. Toulemonde, C. Trautmann, Prog. Nucl. Energy 38 (2001) 281.

[20] K. Richter, A. Fernandez, J. Somers, J. Nucl. Mater. 249 (1997) 121.

[21] J.L. Pouchon, F. Pichoir, in: Electron Probe Quantitation, D.E. Newbury, K.F.J. Heinrich (Eds.), Plenum, New York, 1991, p. 31.

[22] C. Ronchi, C.T. Walker, J. Phys. D: Appl. Phys. 13 (1980) 2175.

[23] J. Magill, Nuclide.net, An Interactive Environment for Computations on Radionuclides and their Radiation, Springer Verlag, 2002. Available at: <www.nuclides.net>.

[24] B.J. Pijlgroms, Burn-up calculations for the EFTTRA T4 experiment, report 21024/99.23088/P, Energieonderzoek Centrum Nederland, 1999.

[25] J.L. Lábár, in: Proc. of EUREM 12, Brno, July 2000, L. Frank, F. Ciampor (Eds.), vol. III, 2000, p. 1379.

[26] W.J. Weber, J.W. Wald, H. Matzke, Mater. Lett. 3 (1985) 173.

[27] I.V. Afanasyev-Charkin, R.M. Dickerson, D. Wayne Cooke, B.L. Bennett, V.T. Gritsyna, K.E. Sickafus, J. Nucl. Mater. 289 (2001) 110.

[28] V. Georgenthum, J. Brillaud, N. Chauvin, M. Pelletier, D. Planck, Prog. Nucl. Energy 38 (2001) 317.
[29] J. Noirot, L. Desgranges, N. Chauvin, V. Georgenthum, J. Nucl. Mater., these Proceedings. doi:10.1016/S0022-3115(03)00177-6.
[30] N. Chauvin, C. Thiriet-Dodane, J. Noirot, H. Matzke, R.J.M. Konings, T. Wiss, R.P.C. Schram, K. Bakker, E.A.C. Neeft, R. Conrad, A. van Veen, T. Yamashita, Synthesis on $MgAl_2O_4$ irradiation results, Report JRC-ITU-TN-2002/39, 2002.
[31] F.C. Klaassen, K. Bakker, R.P.C. Schram, R. Conrad, J. Somers, R.J.M. Konings, J. Nucl. Mater., in press.
[32] J.F. Ziegler, J.P. Biersack, U. Littmark, The Stopping and Range of Ions in Solids, Pergamon, Oxford, 1985.
[33] N. Chauvin, R.J.M. Konings, H. Matzke, J. Nucl. Mater. 274 (1999) 105.
[34] R. Fromknecht, J.-P. Hiernaut, H. Matzke, T. Wiss, Nucl. Instrum. and Meth. B 166/167 (2000) 263.
[35] D.M. Roy, R. Roy, E.F. Osborn, J. Am. Ceram. Soc. 36 (1953) 149.
[36] T.F.M. Barth, Z. Kristallogr. 82 (1932) 325.
[37] T. Yamashita, N. Nitani, H. Kanazawa, M. Magara, T. Ohmichi, H. Takano, T. Muromura, J. Nucl. Mater. 274 (1999) 98.